



Biomechanical Regenerative Braking Energy Harvester: A Systematic Analysis

Kyung-Taek Yoon¹ · Young-Man Choi¹

Received: 19 May 2022 / Revised: 10 August 2022 / Accepted: 12 September 2022 / Published online: 26 September 2022
© The Author(s), under exclusive licence to Korean Society for Precision Engineering 2022

Abstract

Regenerative braking is a well-known technology applied in electric vehicles to achieve high energy efficiency through an energy-recovery mechanism. The same concept has been applied to robotic applications, such as legged robots, lower-limb prostheses, and biomechanical energy harvesters. In particular, a biomechanical energy harvester enables humans to generate watts of power while simultaneously assisting in the braking of human joints during walking. In this study, a systematic analysis of a biomechanical regenerative braking energy harvester was conducted. First, we reviewed the design considerations of each harvester component and designed an energy-harvester prototype with high power density through a systematic design process. Subsequently, the dynamics of the designed harvester and its effect on human biomechanics were analyzed through device testing and human testing. The designed harvester demonstrated a power density of 3.3 W/kg for level-ground walking during device testing. We evaluated muscle activities and joint kinematics in versatile walking scenarios such as sloped walking. In level-ground and downhill walking, the hamstring muscle activity was assisted by the braking torque simultaneously generating 1.2 W and 0.7 W, respectively, during negative work phase. Meanwhile, we confirmed that the braking torque was generated rather in the positive work phase interfering the quadriceps muscle activity. Comparing previous knee-joint-driven biomechanical regenerative braking energy harvesters, our harvester shows relatively high power density level even with slower walking speed and without any special mechanism.

Keywords Energy harvesting · Electromagnetic generator · Regenerative braking · Systematic analysis

1 Introduction

Wearable energy-harvesting technology generates electrical energy based on the kinetic or thermal energy of a human body [1, 2]. As conventional lithium-ion or lithium-polymer rechargeable batteries have limited charge capacity and portability [3], wearable energy-harvesting devices have emerged owing to their advantages of continuous power supply and environment-independent characteristics. Wearable energy harvesters can be classified in several ways, depending on the energy source of the human body and the electrical power generation principle. First, the method of harvesting energy through body temperature mainly involves attaching a thermoelectric or pyroelectric generator to the skin to convert the heat of the human body into electricity

[4]. An electrical power density of 0.45–18 $\mu\text{W}/\text{cm}^2$ can be harvested through this method [5–7]. Another harvesting method uses kinetic energy from the human body. Humans produce a large amount of biomechanical power in their daily lives. In particular, several tens of watts is generated in the lower extremity joints during walking, which is the most frequent activity performed by humans [8]. The piezoelectric [9], triboelectric [10], and electromagnetic [11, 12] energy-harvesting methods are generally applied to harvest the kinetic energy of human motion. These harvesting methodologies generate electrical power of several milliwatts and can be applied as energy sources in self-powered electronic devices or wearable biomedical sensors [13, 14].

Additionally, wearable devices that require high electrical power of several watts also exist. For example, hundreds of watts of electrical power is required to operate tactical devices per soldier in modern warfare [15]. Electrical heating garments, which are clothes designed for outdoor activities in cold weather, require a power of ~10 W [16]. In addition, an electrical energy of ~66 J or an electrical power of

✉ Young-Man Choi
ymanchoi@ajou.ac.kr

¹ Department of Mechanical Engineering, Ajou University, Suwon, Republic of Korea

66 W per single gait cycle is required to actuate a wearable powered exoskeleton or prosthesis [17, 18]. In the field of exoskeletons and prosthetic limbs, energy-efficient mechanisms or actuators have been proposed to reduce driving power. A representative example, compliant actuation, has been realized by adding elastic elements for energy storage and return [19–21], or by connecting elastic elements to actuators, such as in series elastic actuators [22]. In the case of actuators, a high power density is secured through a quasi-direct-drive, which consists of a high-power motor and low-speed transmission [23, 24]. In addition, regenerative braking technology, used in hybrid/electric vehicles and legged robots [25], is being applied to prosthetic lower limbs [26–28].

Regenerative braking has also been applied in wearable energy harvesting for high electrical power generation [29]. As shown in Fig. 1, when the mechanical power of human joints is delivered to the transmission, the joint angular velocity is amplified for generating several watts of power. The generator simultaneously produces electrical power and back-electromotive force (EMF)-based reaction torque. The reaction torque is also amplified through the transmission and acts on the human joint. The harvested electrical power is transmitted to a power management circuit, which rectifies or manages power to be suitable for applications, such as electronic devices or batteries. A controller can switch the generator on/off or adjust the amplitude of the electrical power based on human bio signal information. As the human lower-limb joints propel and brake continuously during the gait cycle, the reaction torque of the harvester was utilized as a braking torque by only operating the harvester in the negative work phase of the lower-limb joint. Specifically, the harvester assists in the deceleration of knee flexor muscles only in the swing extension phase, which requires a large amount of braking torque, using a one-way clutch. Owing to this joint-assisting function during walking, the harvester has recently been called an “energy-harvesting exoskeleton”. The cost of harvesting (COH) and the total cost of harvesting (TCOH) were proposed [29, 30]. The COH is the amount of additional metabolic power required to generate 1 W of electrical power, whereas the TCOH is the metabolic power that reflects not only the harvest cost but also the additional

metabolic power required to carry or wear the harvester. As the metabolic power is efficiently saved in this regenerative braking energy-harvesting technology, a low COH of 0.7 was achieved while harvesting an electrical power of 4.8 W.

After the concept and core mechanism were introduced [29, 30], various biomechanical regenerative braking energy harvesters (BRBEHs) were studied, as shown in Table 1. Most studies have implemented novel functions for the harvester through improved transmission mechanisms. Mechanisms that use a bidirectional gear train [36] or variable transmission [37, 38, 44] to harvest a larger amount of energy or to control the amplitude of the braking torque within a gait cycle have been proposed. Furthermore, a device for harvesting energy while simultaneously assisting both negative and positive work by combining an elastic mechanism has been studied [41, 42]. Finally, the energy harvester was extended from the knee to the ankle joint in some studies [39, 43]. The aforementioned cases were passive types that relied on the movement of the knee using a one-way clutch according to the first prototype concept. To overcome the limitations of the passive type, some studies have attempted energy harvesting optimized for walking through a biosensor-feedback-based control system [34, 35, 45]. As the harvester has been studied continuously, its size and mass have been reduced to increase the power density. Electrical power was harvested from a minimum of 0.3 W to a maximum of 6.5 W during a gait cycle while achieving a COH of -0.56 to 3.9.

An analysis of the structure and mechanism of previous harvesters shows that each harvester has different structural or dynamic characteristics, but similar human joint–transmission–generator–control system configuration. The performance of the harvester is affected not only by the characteristics of each component but also by the combination of components. For example, two combinations of components, namely, a high-power generator with a low transmission ratio [30] and a low-power generator with a high transmission ratio [35], can generate the same amount of electrical power, but other properties of these combinations, such as braking torque and efficiency, are different. In most earlier studies, the concept of BRBEH was proposed and verified through the simplified selection of components with average performance. However, if the design parameters are determined through a systematic design process that reflects the characteristics of each element, a high-end BRBEH can be designed in terms of design and operation. Several parametric studies have been conducted to determine the design values of BRBEHs. In [31], a high-efficiency BRBEH was designed by predicting the device efficiency and electrical power according to the gear ratio. Another study compared the device efficiency of different commercial generators and electrical loads [32]. In other studies, the knee joint torque was predicted according to the change in the spring

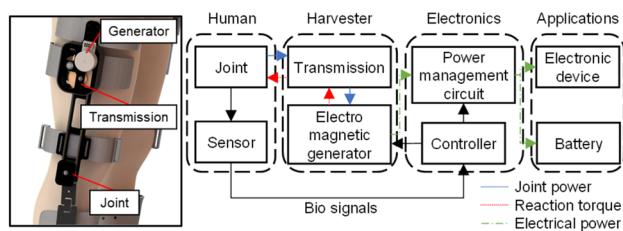


Fig. 1 Block diagram of a biomechanical energy harvester

Table 1 Previous studies on BRBEHs

Study	Target joint (assistance timing)	Gait terrain	Wearing position (Form factor)	Power transmission (Ratio)	Generator constant [V/rad/s]/resistance [Ω]	Control method (negative work selection/reaction torque profile)	Device mass (kg)	Electrical power (W)	COH/TCOH
Li et al. [29, 31]	Knee joint (swing extension)	Level-ground (1.5 m/s)	Directly to joint	Spur-gear train (113)	0.0335/1.03	One-way clutch/delay control with relay switch (5 Ω)	1.6	4.8 ± 0.8	0.7 ± 4.4/–
Shepertyky et al. [30, 32, 33]	Lower limb (Swing extension)	Level-ground (1.5 m/s)	Remote from joint	Spur-gear train (5)	0.027/0.39	One-way clutch/passive electrical load (2.5 to 19 Ω)	2.7	5.2	0.5 ± 2.0/4.0 ± 3.6
Cervera et al. [34]	Knee joint (Swing extension)	Level-ground (1.3 m/s)	Directly to joint	Spur-gear train (83)	0.025/0.41	Gait detection with rotary encoder/torque proportional control with converter	1.5	3–8	–2–5/–
Selinger et al. [35]	Knee joint (All negative work)	Level-ground (0.9 to 2.0 m/s) Uphill/downhill (15°, – 15°)	Directly to joint	Spur-gear train (110)	0.034/–	Gait detection with electromyography sensor/torque proportional control with converter	1.1	1.5–3.5	–
Chen et al. [36]	Knee joint (All swing phase)	Level-ground (1.5 m/s)	Directly to joint	Spur-gear train (106)	0.037/0.608	One-way clutch/passive electrical load (6 Ω)	0.4	3.6	–
Kobayashi et al. [37, 38]	Knee joint (Swing extension)	Level-ground (1.5 to 3.0 m/s)	Directly to joint	Continuously variable transmission (16 to 144)	0.025/1.4	–/Passive electrical load	0.8	0.05 J	–
Cai et al. [39]	Ankle joint (Dorsiflexion)	Level-ground (1.36 m/s)	Directly to joint	Planetary-gear train (159)	0.0224/2.8	One-way clutch/passive electrical load (2.8 Ω)	0.4	0.35 ± 0.02	–2.29 ± 31.9/–
Fan et al. [40]	Knee joint (Flexion and extension)	Level-ground (1.5 m/s)	Directly to joint	Ball screw and pulley wire (39)	0.131/6.89	–/Passive electrical load (75 Ω)	1.85	4.1 ± 0.4	3.9 ± 6.3/8.2 ± 6.0
Xie et al. [41]	Knee joint (Swing extension)	Level-ground (0.91 to 1.5 m/s)	Directly to joint	Spur-gear train (110)	0.04/20	–/Passive electrical load (6 Ω)	0.2	1.2–5.8	–
Xie et al. [42]	Knee joint (Swing extension)	Level-ground (0.91 to 1.5 m/s)	Remote from joint	Spur-gear train (150)	0.01/3	Torsional spring/passive electrical load (3 Ω)	1.7	5.3 ± 0.53	–

Table 1 (continued)

Study	Target joint (assistance timing)	Gait terrain	Wearing position (Form factor)	Power transmission (Ratio)	Generator (generator constant [V/rad/s]/resistance [Ω])	Control method (negative work selection/reaction torque profile)	Device mass (kg)	Electrical power (W)	COH/TCOH
Liu et al. [43]	Ankle joint (Dorsiflexion)	Level-ground (1.3 m/s)	Directly to joint	Winding mechanism (44.5)	0.025/1.24	String and rubber band/passive electrical load (1 Ω)	0.1	0.3	–
Chan et al. [44]	Knee joint (Flexion)	Level-ground (1.1 m/s)	Remote from joint	Gear train and variable-radius drum (3.6 to 14)	0.022/2.95	One-way clutch/passive electrical load (2.5 Ω)	0.48	0.38 \pm 0.046	–/6.31
Shepertyky et al. [45]	Lower limb (Swing extension)	Level-ground (1.25 m/s)	Remote from joint	Spur-gear train (3)	0.0276/0.386	Gait detection with rotary encoder/muscle-centric torque control with converter	1.28	0.25	–0.56/–
Ren et al. [46]	Lower limb (Swing extension)	Level-ground	Directly to joint	Spur-gear train (6)	–/300	Shifting sliding gear/Passive electrical load (700 Ω)	0.32	5.6	–
Wu et al. [47]	Lower limb (Flexion and extension)	Level-ground (1.4 m/s) Downhill (–8°)	Directly to joint	Spur-gear train (72)	0.01/0.5	One-way clutch/passive electrical load (0.5 Ω)	0.54	5.4 (ground) 6.5 (downhill)	–0.006/– (ground) –0.01/– (downhill)

or damping constant of the proposed mechanism [41, 42]. However, previous studies focused only on one or two of the components and did not reflect the comprehensive features of the BRBEH in the design process. To the best of our knowledge, the design considerations for each BRBEH element have not been studied in detail.

In this study, we systematically investigated the BRBEH from two aspects. First, the characteristics and design considerations for each element of the harvester were determined based on an analytical model. Subsequently, we proposed a systematic design process for an energy harvester based on the analysis results. According to the design process, we designed the BRBEH with the goal of maximizing power density. From the second perspective, we conducted an experimental analysis by building an energy-harvester prototype for investigations that could not be reflected in the theoretical model, such as human biomechanics. In particular, the joint kinematics and muscle activities during sloped walking were explored. To the best of our knowledge, previous BRBEHs were designed and tested based on level-ground walking. Experiments on sloped walking were conducted in only two studies [35, 47], but the harvested power and COH were measured without biomechanical or systematic analysis. As the joint mechanics of sloped walking is different from those of normal walking, this analysis can provide design insights to broaden the applicability of BRBEHs.

2 Analysis of the Energy-Harvesting System

Figure 2 shows the structural configuration of the BRBEH system. There are two representative form factors of BRBEHs depending on the wearing positions as shown in Table 1. Most previously studied BRBEHs had a “hard-type” structure, which is directly fastened to the joint with rigid frames. In this structure, the braking torque or force of the harvester will be delivered accurately, but wearability may

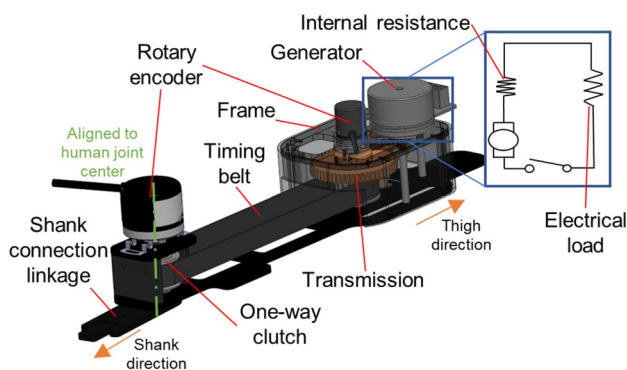


Fig. 2 Structural configuration of the BRBEH

be reduced. To overcome this problem, the form factor of the soft exoskeleton has been reflected, and this “soft-type” structure allows the harvester to be worn remotely from the joint [30, 42, 44, 45]. In contrast to the hard-type structure, the force or torque may not be transmitted accurately. The prototype in this study was designed to be directly connected to the joint, according to the most widely used hard-type form factor. We attempted to minimize the metabolic penalty owing to the carrying of a mass by arranging the main elements of the harvester close to the pelvis, which is close to the center of gravity of the human body, using a timing belt, like in remote cable-driven harvesters [48].

The prototype mainly consists of a timing belt, three-stage spur-gear train transmission, and generator. The transmission and generator are placed near the thigh side in a compact arrangement. On the shank side, a one-way clutch is installed on the input shaft to transmit the knee joint power only during knee extension. The timing belt connects the shank and thigh sides. The working principle is the same as that of the general BRBEH described above. When knee motion is input to the shaft aligned with the knee joint, it is transmitted via the timing belt to the transmission and generator. Electrical power is then generated from the generator, and the braking torque is transmitted back to the knee joint through the transmission and timing belt.

2.1 Analytical Model of the Energy Harvester

When a human joint runs an energy harvester, the human joint velocity (ω_h) is delivered to the one-way clutch and the transmission. As most previous studies adopted a passive one-way clutch as the negative work selection method of joints, a harvester equipped with a transmission based on a one-way clutch is proposed as a general model. Through a one-way clutch, the input transmission velocity (ω_t) is amplified by the transmission ratio (r_t) and is transmitted to a generator.

$$\omega_g = r_t \cdot \omega_t, \quad (1)$$

where ω_g denotes the generator velocity. The generator produces a back-EMF voltage E proportional to its own velocity.

$$E = K_g \cdot \omega_g, \quad (2)$$

where K_g denotes the generator constant. The induced electric current in the generator (I_g) is determined by the internal resistance of the generator (R_g) and the electrical load of the external circuit (R_L).

$$I_g = \frac{E}{R_g + R_L}. \quad (3)$$

The harvested voltage (V_L) and electrical power (P_E) are the values of the electrical load as follows:

$$V_L = I_g \cdot R_L, \tag{4}$$

$$P_E = \frac{V_L^2}{R_L}. \tag{5}$$

The generator torque (τ_g) from the generator is related to the generator constant and the induced current as follows:

$$\tau_g = K_g \cdot I_g. \tag{6}$$

The reaction torque (τ_r) is the amplified generator torque through the transmission, which is then applied to the human joint.

$$\tau_r = \frac{\tau_g \cdot r_t}{\eta_t}, \tag{7}$$

where η_t denotes the transmission efficiency. By substituting Eqs. (1), (2), (3), and (6) into (7), the reaction torque can be expressed in terms of the transmission velocity.

$$\tau_r = C_g \cdot \omega_t, C_g = \frac{(K_g \cdot r_t)^2}{\eta_t \cdot (R_g + R_L)}, \tag{8}$$

where C_g denotes the damping constant provided by the generator [43]. In addition to the reaction torque from the generator, there is inertia torque in the harvester. The overall inertia of the energy harvester consists of two main parts: the generator inertia (J_g) and transmission inertia (J_t). Inertia appears differently depending on the specific location. To describe the inertial torque applied to the user, the equivalent inertia (J) of the input shaft is expressed as follows:

$$J = J_t + r_t^2 \cdot J_g. \tag{9}$$

The inertia torque applied to the user is defined as follows:

$$\tau_i = J \cdot \dot{\omega}_t. \tag{10}$$

There are other reaction torque components, such as friction torque, but they are not included in this model because there are various models depending on the design. The total braking torque (T) exerted on the user is expressed as

$$T = \tau_r + \tau_i = C_g \cdot \omega_t + J \cdot \dot{\omega}_t. \tag{11}$$

The mechanical power of the harvester (P_M) is the product of the total torque and the angular velocity of the transmission:

$$P_M = T \cdot \omega_E. \tag{12}$$

The device efficiency (η_d) of the energy harvester can be defined as follows:

$$\eta_d = \frac{P_E}{P_M} = \frac{V_L^2/R_L}{(\tau_r + \tau_i) \cdot \omega_t}. \tag{13}$$

The relationship between the angular velocity of the human joint and transmission velocity is determined by the engagement condition of the one-way clutch, as shown in Fig. 3. In the engagement condition, the transmission velocity is determined by the angular velocity of the human joint multiplied by the mechanical coupling efficiency (η_c), which reflects the velocity loss, as shown in Eq. (14). There is a possibility of imperfect delivery of the joint motion to the transmission owing to joint misalignment between the harvester and the human joint, or the structural deformation of the cuff or brace connecting the human body and the harvester. Under the disengagement condition, the velocity of the human joint is not delivered to the harvester, and the braking torque of the harvester is not transmitted to the human joint. At this time, the velocity of the transmission decays exponentially, as shown in Eq. (15).

$$\text{Engagement : } \omega_t = \eta_c \cdot \omega_h, \tag{14}$$

$$\text{Disengagement : } \omega_t = \omega_0 e^{-\frac{C_g}{J}(t-t_0)}, \tag{15}$$

where ω_0 and t_0 represent the velocity of the transmission and the time at which disengagement occurs, respectively.

The engagement and disengagement thresholds are as follows [43]:

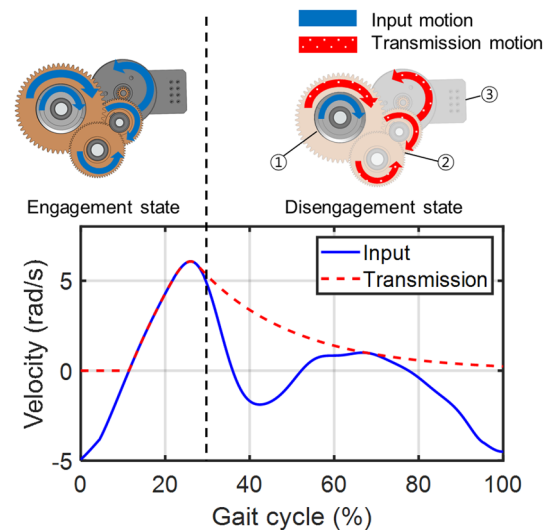


Fig. 3 Schematics and velocity comparison of the engagement and disengagement conditions of the one-way clutch. The components in the schematics are labeled as follows: ① one-way clutch, ② transmission, and ③ generator

$$\text{Engagement} : \omega_t = \eta_c \cdot \omega_h \text{ and } -\frac{C_g}{J} \leq \eta_c \cdot \dot{\omega}_h, \quad (16)$$

$$\text{Disengagement} : \omega_t > \eta_c \cdot \omega_h \text{ or } -\frac{C_g}{J} > \eta_c \cdot \dot{\omega}_h. \quad (17)$$

Disengagement occurs when the angular velocity of the transmission is higher than that of the input part, owing to the overrunning effect from the inertia of the transmission. By contrast, the acceleration of the human joint should be higher than the time constant (C_g/J) of the transmission to maintain the engagement.

2.2 Biomechanics of the Human Lower-limb Joint

The dynamics of human gait should be carefully considered to implement the BRBEH technology effectively. The amplitude of the negative power of the joint should be sufficiently high to require braking assistance. The range of motion (RoM) of the joint in the negative work phase is also an important factor. As the generation power and braking torque amplitude of an electromagnetic generator are proportional to the input velocity, as shown in Eqs. (2) and (8), securing a high RoM has greater potential for the practical usage of BRBEHs. Finally, there should be a substantial contribution of the muscle to the negative work of the joint. Unlike positive work, passive elements, such as ligaments, also contribute to the work in addition to muscles in the negative work of the joint [49]. As passive elements do not require metabolic energy, braking assistance with an energy harvester would be less effective if the negative work contribution of the passive elements of the joint is equal to or greater than that of the muscles.

In level-ground walking, the knee joint is responsible for most of the negative work during the gait cycle; hence, most previous energy harvesters were operated based on knee joint motion. In particular, the swing extension phase of the knee joint has been adopted as a generation phase because of the wide RoM and the practical use of the hamstring muscles for negative work. In some studies, the negative work of the ankle joint was utilized [39, 43]; however, the harvested electrical power was lower than that of knee-joint-based harvesters because the RoM of the ankle joint is relatively narrower than that of the knee joint. As the hip joint has less than 20% of the negative work section during gait, this joint was not used.

However, caution should be exercised when applying the same assisting strategy in other gait environments because the biomechanics of joints are different from those in level-ground walking. A typical example is sloped walking [50]. In the case of uphill walking, a significant amount of positive work to propel the body upward occurs at all joints, whereas

the portion of negative work decreases significantly. Thus, even in the case of the knee joint, regenerative braking can be an energetic penalty. For example, knee swing extension, which is the optimal period for regenerative braking on level ground, is undesirable because it is a positive work phase in uphill walking. Therefore, even if a small amount of biomechanical energy is harvested compared with that in level-ground walking in the same gait phase, the COH may be higher during uphill walking. Conversely, in downhill walking, a significant amount of potential energy is absorbed by the muscles, and the negative work portion increases at all joints. Thus, for the knee joint, a harvesting strategy similar to that for level-ground walking can be adopted because the knee joint produces three times more negative power [50]. In addition, the energy storage capacity of the ankle joint increases during downhill walking, resulting in a greater fraction and amplitude of negative work. Therefore, the harvester can support the negative work of the ankle joint more effectively than that during level-ground walking. Other physiological characteristics, such as muscle activity or joint kinematics on sloped walking, other than the joint perspective view, will be described later in the experimental analysis. Although our study focused on sloped gait, other gait conditions, such as running or squatting, also exist and may be considered.

2.3 Energy-Harvester Components

As previously mentioned, the configurations of all previous energy harvesters can be divided into three main parts: transmission, generator, and control system. In this section, the main roles and important design considerations for each element are analyzed.

2.3.1 Transmission

The transmission amplifies the human joint angular velocity and braking torque. The core design parameters are the transmission ratio (r_t) and inertia (J_t). If the transmission ratio is too low, the harvester generates a small amount of electricity. By contrast, an excessively high transmission ratio generates excessive reaction torque that impedes walking. This also reduces the transmission efficiency. The inertia of the BRBEH plays two primary roles. First, the inertia drives the generator similar to a flywheel, enabling continuous energy generation. Moreover, the inertia torque is applied to the knee in addition to the reaction torque. If the intensity of the inertial torque is high, an inordinate braking torque may act, and the amount of power generation may need to be adjusted to prevent this phenomenon. The transmission inertia contributes to the generation of inertia torque in the harvester. However, as shown in Eq. (9), the inertia of the generator is amplified by the square of the

transmission ratio and shows more dominant characteristics. Thus, it is beneficial to adjust the transmission ratio and generator inertia, rather than the transmission inertia, to control the inertial torque. Structurally, the transmission usually determines the mass and volume of the harvester; therefore, it is necessary to design the transmission to be compact and lightweight. Most harvesters adopt the traditional spur-gear train structure, and there are cases in which cables or spring mechanisms are applied for more effective energy harvesting.

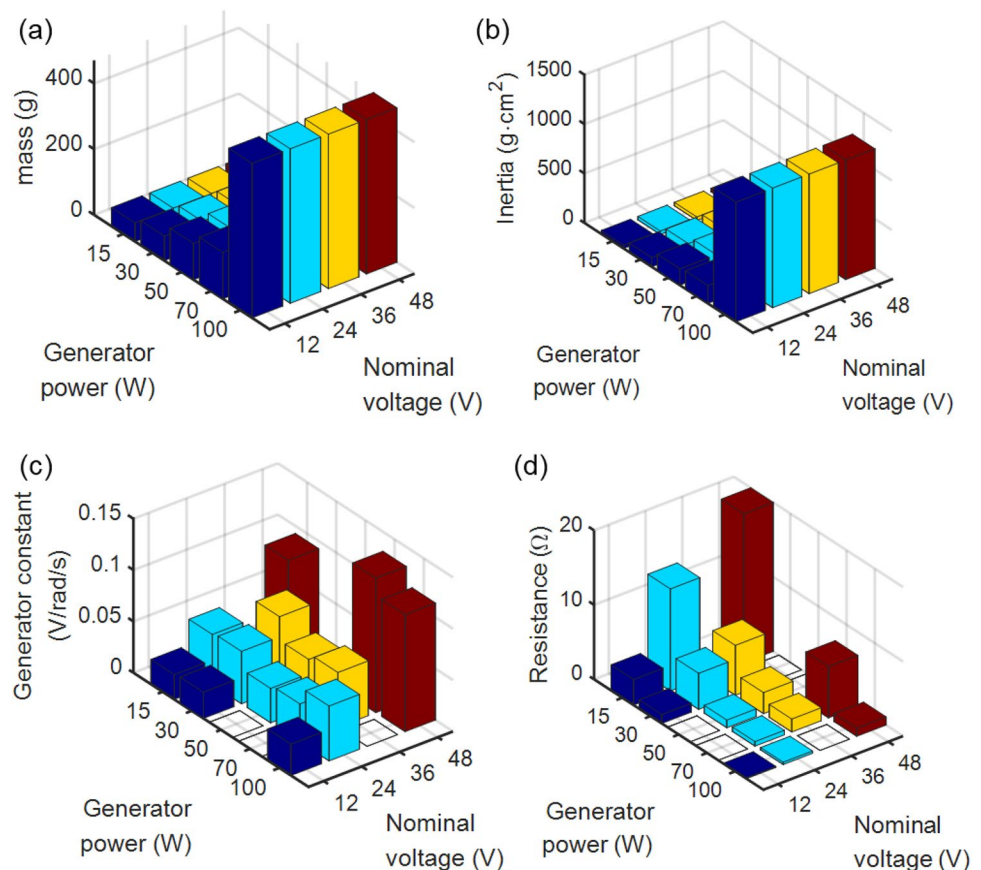
2.3.2 Generator

As a source of electrical power and braking torque, a rotary electromagnetic generator must have a high power density, high efficiency, and compact structure. Designing a generator specifically for the BRBEH may be the best choice to achieve these properties. However, to save time and cost, commercial three-phase brushless DC (BLDC) motors with flat structures were used as generators in all previous harvesters. Therefore, in this study, the characteristics of the generator were identified based on the parameters of a commercial BLDC generator.

Figure 4 shows a graph summarizing the mechanical and electrical parameters of commercial generators with respect

to their rated power and nominal voltage [51]. These generators have a realistic range that does not exceed the rated torque and voltage when combined with a generator-independent variable, and hence, they have been widely applied in the previous studies [29, 30, 34, 36, 40]. The mechanical properties of inertia (J_g) and mass in Figs. 4a, b, respectively, increase rapidly as the generator has larger power capacity. The nominal voltage does not affect the mechanical properties of the generator. Thus, if a high-power generator is used, the penalties of mass and inertia must be considered, despite the benefits of electrical power. The electrical characteristics of the generator are shown in Figs. 4c, d. The generator constant (K_g), which is a proportionality constant between the EMF and rotation speed, had no significant correlation with the power of the generator. The internal resistance (R_g) of the generator decreases as the rated power increases, because thicker copper wires are used to withstand the higher current in the high-power generator. The generator constant and internal resistance increase simultaneously as the nominal voltage increases. This is because a generator with a high nominal voltage has thin wires with several turns, whereas low-nominal-voltage generators are made with thick wires and few turns. From the viewpoint of power generation, it is advantageous to use high-nominal-voltage generators with high generator constants. Although the output current and

Fig. 4 Comparison results of commercial generators according to the generator power and nominal voltage; **a** mass, **b** inertia, **c** generator constant, and **d** internal resistance. An empty space without a bar indicates that the combination does not exist



braking torque decrease as the internal resistance of the generator increases, this can be compensated by adjusting the external electrical load (R_L), as shown in Eqs. (3) and (8). Finally, for stable operation, the generated current should not exceed the maximum continuous current of the generator during harvesting.

2.3.3 Control System

Unlike other harvesters that focus on efficiently storing and managing harvested electricity, the BRBEH control system has two essential roles: (1) selectively activating the harvester by detecting the negative work of the human joint during the gait cycle and (2) controlling the braking torque profile. In the first method of selecting the negative work of a human joint, the most representative method involves selecting the work passively according to the motion direction of the joint using mechanical components or mechanisms. This method can be implemented simply without a complex gait detection algorithm; however, it lacks sophistication and cannot respond to changes in the walking environment. Some studies have implemented algorithms to detect the gait cycle through biosensor-based feedback and select a negative work phase based on the gait cycle in the controller [34, 35, 45]. Based on the selected negative working phase, the harvester is electrically controlled on/off, and electrical power is harvested in all negative work phases, offering more negative work support compared with mechanical passive control. The second function was to control the braking torque profile. The optimal braking torque profile for each human joint remains an open issue. Recently, a strategy to generate braking torque by subtracting the torque generated through passive elements from the joint torque was proposed, and it showed excellent braking assistance for human joints [45]. Therefore, generating an optimal braking torque profile is key to reducing the COH during harvesting. According to Eq. (8), there are two methods for controlling the torque profile: changing the transmission ratio and changing the electrical load value according to the gait cycle. First, in the case of changing the transmission ratio, mechanical systems, such as continuously variable transmission [38] and variable-radius drums [44], were adopted. This method has a higher efficiency than the electrical control method; however, the mechanism becomes more complicated and may not respond immediately. The second method involves changing the electrical load through a converter circuit [34, 35, 45]. In this case, a fast response is possible, and a more sophisticated torque profile can be created. However, the energy losses can be higher than those of the mechanical systems. For simplicity, in most studies, harvesting was performed without changing the transmission ratio and electrical load during the gait cycle. In this case, the torque profile was proportional to the angular velocity of

the joint. In addition, by selecting a load equal to the resistance of the generator, maximum power transfer was achieved [39, 42, 43, 47]. In terms of harvesting power, this passive electrical load method may be sufficient; however, torque profile control is essential for a more advanced BRBEH.

Finally, power electronic circuits for managing and storing harvested power with the maximum efficiency are required for BRBEHs. As only one study on power electronics has been conducted [52], it is not discussed in this paper. However, to minimize the COH, the use of power electronics should be considered as an important control method to minimize metabolic energy.

3 Design Process of Energy Harvester

In this section, a BRBEH is designed through a systematic design process that can determine design parameters based on a comprehensive observation of the performance of the harvester according to the characteristics of the harvester components. Notably, the suggested design procedure selects a commercial generator, rather than designing a custom generator according to the trends of previous studies.

Figure 5 shows a flowchart of the systematic design process of the BRBEH. First, the design goals, given conditions, constraints, and design variables were selected. Candidates

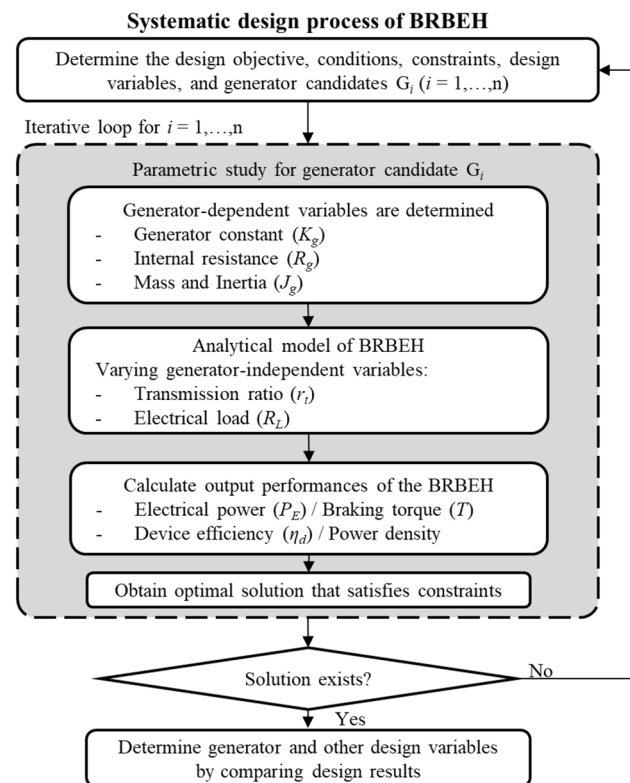


Fig. 5 Flowchart of the systematic design process of the BRBEH

for commercial generators were selected at this stage. Subsequently, a parametric study was performed for each generator candidate. The generator-dependent variables were predetermined to a single value concurrently with the candidate selection. Using an analytical model of the BRBEH, the performance of the harvester was calculated by varying the generator-independent variables, such as the transmission ratio and electrical load. The optimal solution that best satisfies the design objective within the constraints was obtained for each generator candidate. If a solution exists, the final generator and design variables are determined by comparing the design results for each generator. In the absence of a satisfactory solution, the design variables and constraints should be adjusted.

Table 2 summarizes design objectives, in addition to the design variables, given conditions, and constraints. The design objective was to maximize the power density, which is the harvested electrical power divided by the system mass (m_s). The design variables were set as the generator constant, internal resistance, transmission ratio, and electrical load. The generator constant and internal resistance values were determined using a commercial generator. The seven 50 and 70 W commercial BLDC motors introduced earlier were selected as generator candidates for use in the design process. The specifications of each motor is summarized in Table S1 [51]. In studies using these generator candidates or other generators with similar specifications, values ranging from 39 to 113 for the transmission ratio and 1–75 Ω for the electrical load were used. Reflecting these ranges, the design ranges of the transmission ratio and electrical load were set to 30–120 and 1–20 Ω , respectively. Although the maximum load was lowered to 20 Ω , the characteristic change in the harvester according to the change in the electrical load could be sufficiently observed.

As a condition, a harvester system with a fixed transmission ratio and constant load of an electrically passive type was adopted. The harvesting period in the gait cycle was set as the knee swing extension with a one-way clutch while walking on level ground, and the general knee joint angle profile with a walking speed of 1.2 m/s for a healthy adult was applied to the model [53]. It is assumed that the knee joint angle profile is unaffected by the braking torque of the harvester. As the mass and inertia of the transmission are proportional to the transmission ratio, they were set as increasing quadratic functions according to the transmission ratio. The range of inertia was 0.02 to 0.26 kg m², and the range of mass was 1–4 kg. As a constraint on harvester performance, the maximum generated braking torque was limited to 7 N·m, which is half the knee joint torque, so as not to interfere with walking [31]. The maximum generated voltage was set to 30 V because rectification is difficult when the voltage is too high. The minimum harvested power per gait cycle was set to 2 W for meaningful harvesting. Finally, the minimum device efficiency was set to 0.8.

Figure 6 shows the results of the systematic design process according to the transmission ratio and electrical load for generator G4 among the generator candidates. As depicted in Figs. 6a, b, as the transmission ratio increased, the electrical power and braking torque increased, and they had a reciprocal relationship with the electrical load. The generated voltage in Fig. 6c was insensitive to the change in the electrical load and had a linear relationship with the transmission ratio. The device efficiency was unaffected by the transmission ratio and had a logarithmic relationship with the electrical load as shown in Fig. 6d. This is because the efficiency of the transmission was set to a constant value, and only the efficiency of the electric circuit changed according to the electrical load. If the

Table 2 Design objective, variables, conditions, and constraints for energy-harvester design

Design objective	Maximize power density
Design variables	Generator constant (K_g) Internal resistance (R_g) Transmission ratio ($32 < r_t < 120$) Electrical load ($1 < R_L < 20$)
Given conditions	Generation phase: knee swing extension with one-way clutch Terrain: level ground System mass (kg): quadratic function of transmission ratio ($1 < m_s < 4$) Transmission inertia (kg·m ²): quadratic function of transmission ratio ($0.02 < J_t < 0.26$) Transmission efficiency (η_t): 0.95 Mechanical coupling efficiency (η_c): 0.9
Constraints	Braking torque (T) < 7 Nm Generated voltage (V_L) < 30 V Harvested electrical power (P_E) > 2 W Device efficiency (η_d) > 0.8

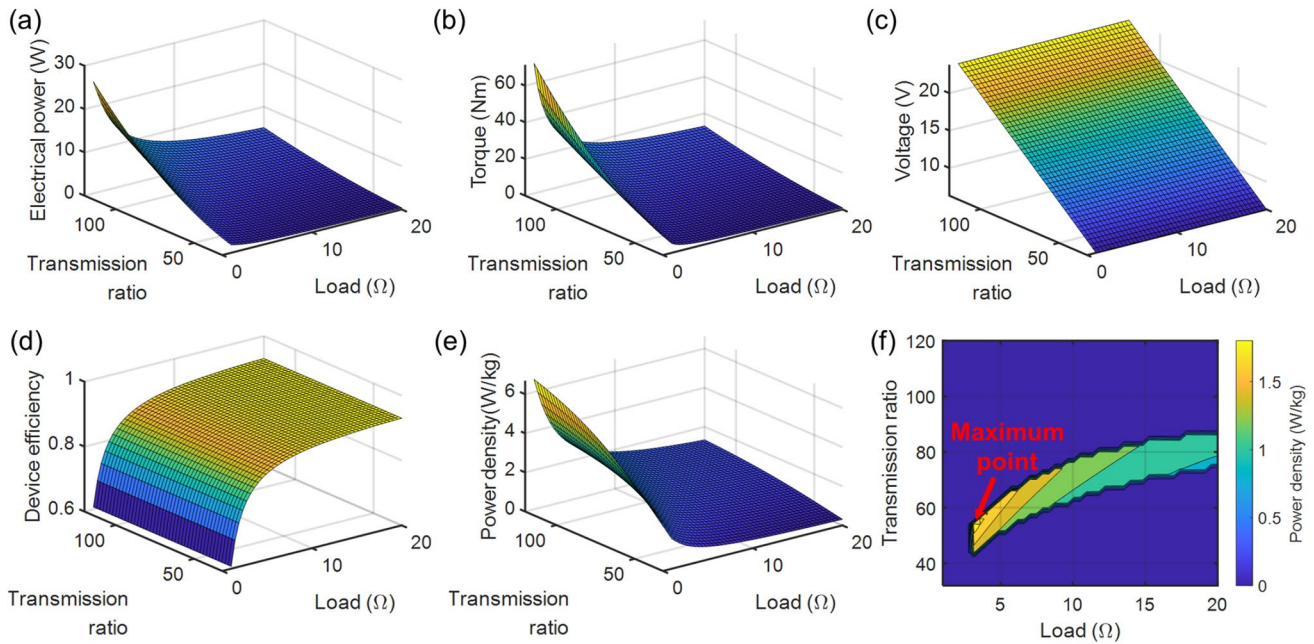


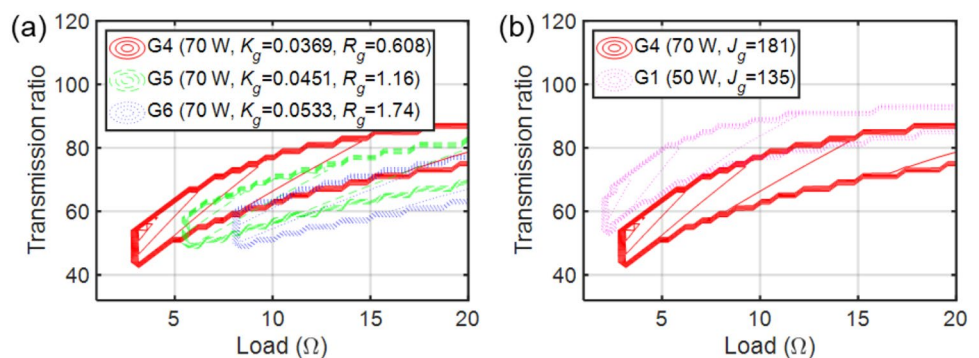
Fig. 6 Parametric analysis for generator G4 according to the transmission ratio and electrical load; **a** electrical power, **b** braking torque, **c** generated voltage, **d** device efficiency, **e** power density, and **f** available design area

transmission efficiency changes considerably according to the input torque, this aspect should be reflected in the model. The power density is shown in Fig. 6e. Owing to the mass penalty for a high transmission ratio, the change in the power density according to the transmission ratio became more gradual compared with that of the electrical power. Figure 6f shows a power density contour plot of the BRBEH, which satisfies the design constraints. Areas that violate the constraints are colored in blue and located above and below the design area. The reason for the limitation of the upper area was the generation of an excessively high braking torque. When the transmission ratio was too high, the maximum value of 7 N·m was exceeded owing to the increase in the inertia torque even though the torque of the generator was decreased by lowering the generated current by increasing the electrical load. The

lower limiting area indicated that the generated power was too low.

For generators other than G4, the designable area showed a similar pattern according to the generator-independent design variables; however, the boundary between the upper and lower restricted areas differed depending on the characteristics of the generator. First, the change in the available design area according to the electrical properties of the generator was confirmed as shown in Fig. 7a. In this case, the mechanical properties were identical for each generator. As the generator constant increased, a BRBEH that satisfied the constraint using a lower transmission ratio could be designed, resulting in an increasing efficiency and power density. Therefore, it is recommended that this aspect be actively utilized by selecting a generator with a high generator constant. However, the upper limit of the transmission

Fig. 7 a Comparison of the design results depending on the generator constant (V/rad/s) and internal resistance (Ω). **b** Comparison of the design results depending on the inertia of the generator (g cm²)



ratio was lowered concurrently to satisfy the maximum braking torque constraint. The internal resistance affected the left boundary of the design area. As the internal resistance increased, the electrical load was increased to satisfy the device efficiency constraint.

In contrast to the previous case, the design results of the harvester were compared by changing the mechanical property of the generator, as shown in Fig. 7b. The generator constants and internal resistances of generators G1 and G4 were similar; however, their inertias were significantly different owing to the rated power. In a generator with high inertia, a lower transmission ratio is required to satisfy the maximum braking torque constraint. The amount of harvested electrical power and braking torque from the generator were similar when the generators had similar electrical characteristics. However, as mentioned earlier, the inertia of the generator plays a decisive role in producing the inertia torque. Thus, it is preferable to select a generator with low inertia to increase the ratio of the generator torque to the inertia torque of the BRBEH.

Finally, the design variables were determined based on the results of the design comparison. Table 3 presents the optimal design results, in which the power density for each generator was maximized. To maximize the power density, the design results tended to have a minimum transmission ratio within the range that satisfied the constraints. No design results satisfied the constraints for the G3 and G7 generators. These generators have a much higher generator constant and internal resistance than the other generators; hence, a gear ratio of 40 or less is required to satisfy the braking torque. Simultaneously, the electrical load had to be sufficiently high owing to the efficiency constraints. Unfortunately, this case did not generate the minimum required electrical power. As a final design result, a G4 generator with a transmission ratio of 54 and an electrical load of 3.2Ω with the highest power density was selected. The predicted power density with this model was 1.95 W/kg , and the generated power per gait cycle was 3.07 W .

4 Experimental Analysis of the Energy Harvester

4.1 Fabrication and Testing Protocol

In the experimental analysis, the physical characteristics of the harvester and their effect on human biomechanics during the gait cycle were analyzed. The prototype was built according to the design results, as shown in Fig. 8a. For convenience, the transmission ratio was slightly adjusted from 54 to 56. The frame and gear were made of an aluminum alloy. The total mass of the system was 610 g , and including braces made of 3D-printed thermoplastic polyurethane, it was 980 g . As shown in Fig. 8b, two braces were installed on the thigh, and one was installed on the shank. The brace worn on the shank was attached as close as possible to the foot to increase the moment arm.

The test bed was set up to analyze its quantitative performance and dynamic characteristics as shown in Fig. S1. In the test bed, BRBEH prototype is driven by the emulating servo motor that simulated the motion of the knee joint. After the test bed was set up as described in Supp. S1, the braking torque and electrical power generated during the operation of the harvester were evaluated. For performance evaluation according to the walking

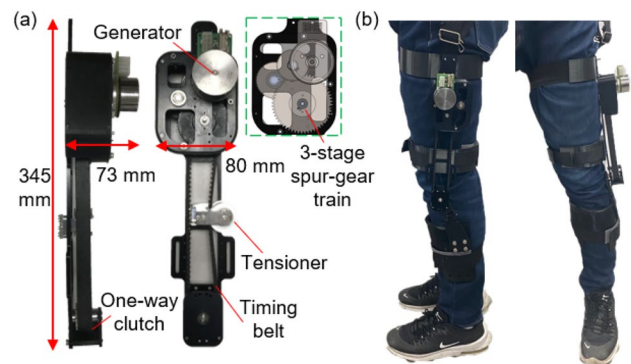


Fig. 8 **a** Fabricated energy-harvester prototype, and **b** view of the device worn by the user

Table 3 Optimal design results for each generator

Generator	Gear ratio	Electrical load (Ω)	Power density (W/kg)	Electrical power (W)	Maximum braking torque ($\text{N}\cdot\text{m}$)	Device efficiency
G1	64	2.3	1.57	2.84	6.76	0.81
G2	68	4.9	1.43	2.74	6.76	0.80
G4	54	3.2	1.95	3.07	6.77	0.82
G5	58	5.8	1.75	2.91	6.66	0.81
G6	60	8.3	1.74	2.98	6.90	0.80

*Solution did not exist in case of G3 and G7 generator

environment, knee joint motion profiles were applied to the emulator for walking on flat ground with a walking speed of 1.2 m/s and for uphill/downhill walking at a speed of 0.47 m/s and an inclination of 30° [53]. To check the behavior of the harvester depending on the electrical load, the experiment was performed by increasing the electrical load from 5 to 20 Ω in steps of 5 Ω , although the designed value was 3.2 Ω . In addition to these four cases, no-load conditions, where the electrical load was not connected, were added to the experimental conditions.

In the human experiment, we focused on how the braking torque of the harvester affected human kinematics and muscle activities through motion capture cameras and surface electromyography (EMG) sensors as shown in Fig. S2. Four healthy male subjects (age: 27 ± 3 years, height: 180 ± 5 cm, weight: 80 ± 1 kg, mean \pm standard deviation) participated in the experiment. The experimental conditions were as follows: (1) no-device state, in which the harvester was not worn, (2) no-load state, and (3) four different electrical loads connected as described above. As with the device testing, three walking terrains were established: level-ground, uphill, and downhill walking. The walking speeds were 1.2 and 0.97 m/s in level-ground walking and sloped walking, respectively, and the slope was 10° . Detailed experimental protocol was introduced in Supp. S2. The protocol was approved by the Institutional Review Board of Ajou University.

4.2 Device Testing

Figure 9 shows the results of device testing for each walking condition. Based on the angular velocities observed with the encoders, a transmission delay and overrunning occurred from the one-way clutch. For the angular velocity, indicated in the first row of the graph, the blue line is the reference knee joint profile and is identical to the profile applied to the input shaft of the harvester. The other line represents the velocity of the transmission passing through the one-way clutch. Unlike the model, a delay of approximately 0.2 s was observed when the transmission was engaged or disengaged. This can be caused by the delay angle of the mechanical clutch [54]. The one-way clutch utilized in this study has a gap of 1° – 2° between the inner and outer rings, and it takes time for the rock to wedge between the inner and outer rings. This is called the delay angle, which depends on the torque capacity and the number of repetition cycles of the one-way clutch. In most previous studies using one-way clutches, it was not possible to determine whether these characteristics occurred because the velocity was not measured. Only one study analyzed the dynamic characteristics [32]; however, in this case, delay and overrunning were not observed. It could be attributed to the unique characteristics of each commercial one-way clutch and differences in the BRBEH design parameters. The second phenomenon, caused by the one-way clutch, is overrunning, in which the velocity of the transmission becomes higher than the input velocity. This is because the transmission continues to maintain a high velocity owing to the flywheel effect after disengagement

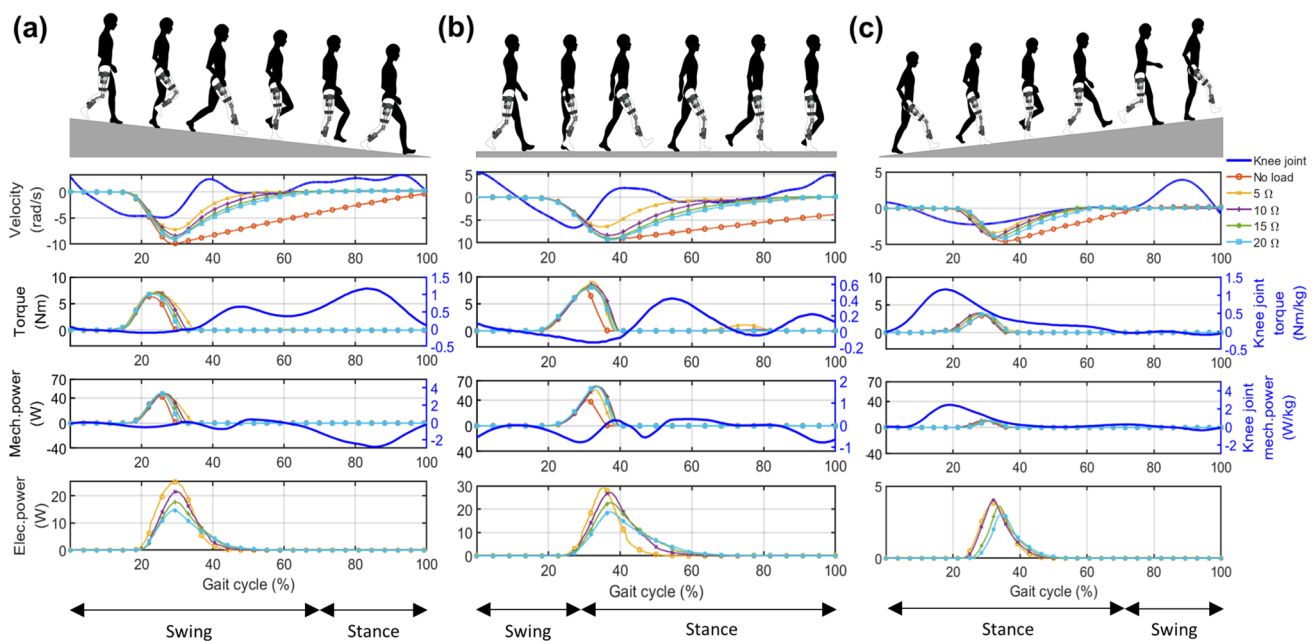


Fig. 9 Device testing result; **a** downhill walking, **b** level-ground walking, and **c** uphill walking

from the input shaft. When the one-way clutch was removed and tested, both characteristics disappeared.

The characteristics of delay and overrunning owing to the one-way clutch require several points to be considered in the harvester modeling and operation. Effective deceleration is only possible when the correct timing is provided within a gait cycle of the human body; thus, for more efficient harvesting, evaluating the one-way clutch delay timing carefully through human testing is required. In the case of overrunning, the advantage is that a higher power can be produced within the gait cycle than that with the knee joint velocity profile. However, the timing of disengagement caused by overrunning should be carefully considered. After disengagement occurs, the braking torque of the harvester cannot be transmitted to the knee joint, and thus, braking assistance may not be achieved as intended. In addition, if the flywheel effect is too strong, the generator continues to run until the next gait cycle, thereby affecting the next braking assistance.

The torque profile of the harvester was applied to the joint peaked at the time of disengagement. The differences in the maximum torque according to the change in the electrical load were insignificant owing to the nearly identical disengagement timings. The measured total braking torque for level-ground walking was approximately 8 N·m. The average generator torque and inertia torque estimated through the generator velocity and modeling were 2.3 and 5.3 N·m, respectively. The remaining torque component was the friction torque generated by the belt or frame, which was approximately 2 N·m. The ratios of the three torque components were the same for the other walking conditions, as listed in Table S2. The high inertia torque and friction torque resulted in a system efficiency of 0.6, which was lower than expected. The electrical loss from the rectifier circuits may also have contributed to the reduction in the device efficiency.

Braking assistance was performed in the swing extension phase, in which the knee joint performed negative work, similar to that in previous studies on level-ground walking, even with the occurrence of a delay effect. In addition, the braking torque was generated at an appropriate time in downhill walking, where negative work was performed in the swing extension phase. However, in downhill walking, the negative work of the knee joint was the largest in the stance flexion phase, which accepts the body mass [50]. Owing to the unidirectional nature of the one-way clutch, the harvester did not drive during flexion. Thus, the opportunity to harvest more power and assist in the negative work of the knee joint was missed. Additionally, during uphill walking, the harvester generated braking torque in the positive power phase, hindering body propulsion.

The average generated powers were 3.2, 0.4, and 2.5 W for level-ground, uphill, and downhill walking, respectively. Furthermore, the average power densities of the harvester

were 3.3, 0.3, and 2.6 W/kg for level-ground, uphill, and downhill walking, respectively. The system was built to be lighter than the weight specified in the modeling, resulting in a slight increase in power density compared to the design result. As the gait speed for level-ground walking was approximately twice that for sloped walking, the harvested powers from level-ground walking and sloped walking cannot be directly compared. When comparing the power generation during uphill and downhill walking, lower power was generated during uphill walking because of the lower knee joint acceleration than that during downhill walking. In terms of both the generation timing and power, a harvester equipped with a one-way clutch is not suitable for sloped walking, and a system that can respond more adaptively according to the walking environment is required.

4.3 Human Testing

The kinematics and muscle activities did not show any significant difference with the change in the electrical load. The device testing results showed that adjusting the electrical load was less effective in altering the braking torque. Thus, the result obtained when an electrical load of 15 Ω was applied was selected as the representative result. The average powers harvested during the experiment were 1.2 ± 0.36 , 0.2 ± 0.07 , and 0.7 ± 0.22 W for level-ground, uphill, and downhill walking, respectively. The maximum braking torques estimated by the analytical model were 4, 2.6, and 3.2 N·m for level-ground, uphill, and downhill walking, respectively. Compared with device testing, approximately three times lower electrical power was harvested. Owing to this power loss, the power densities of the harvester were reduced to 1.2, 0.2, and 0.7 W/kg, respectively, for level-ground, uphill, and downhill walking. The reason for the reduced electrical power was a decrease in the knee joint RoM owing to the braking torque, as shown in the kinematics results described later. In addition, the instantaneous center of rotation of the knee changes according to the rolling and sliding motions between the tibia and the femur [55]. However, the designed harvester did not reflect the kinematic characteristics of the knee, resulting in reduced mechanical coupling efficiency (η_c).

Figure 10 shows the kinematics of the lower-limb joints according to the harvester operation for each gait condition. As the designed harvester does not interfere with the ankle joint structurally, statistical significance via a paired t-test of the ankle joint RoM was not observed compared with the no-device condition, as shown in Table S3. The knee joint showed a significant difference ($p < 0.05$) between the no-device condition and walking with braking assistance during sloped walking. There was no statistical difference in level-ground walking, but the RoM of the knee decreased numerically. The knee was less extended in swing extension

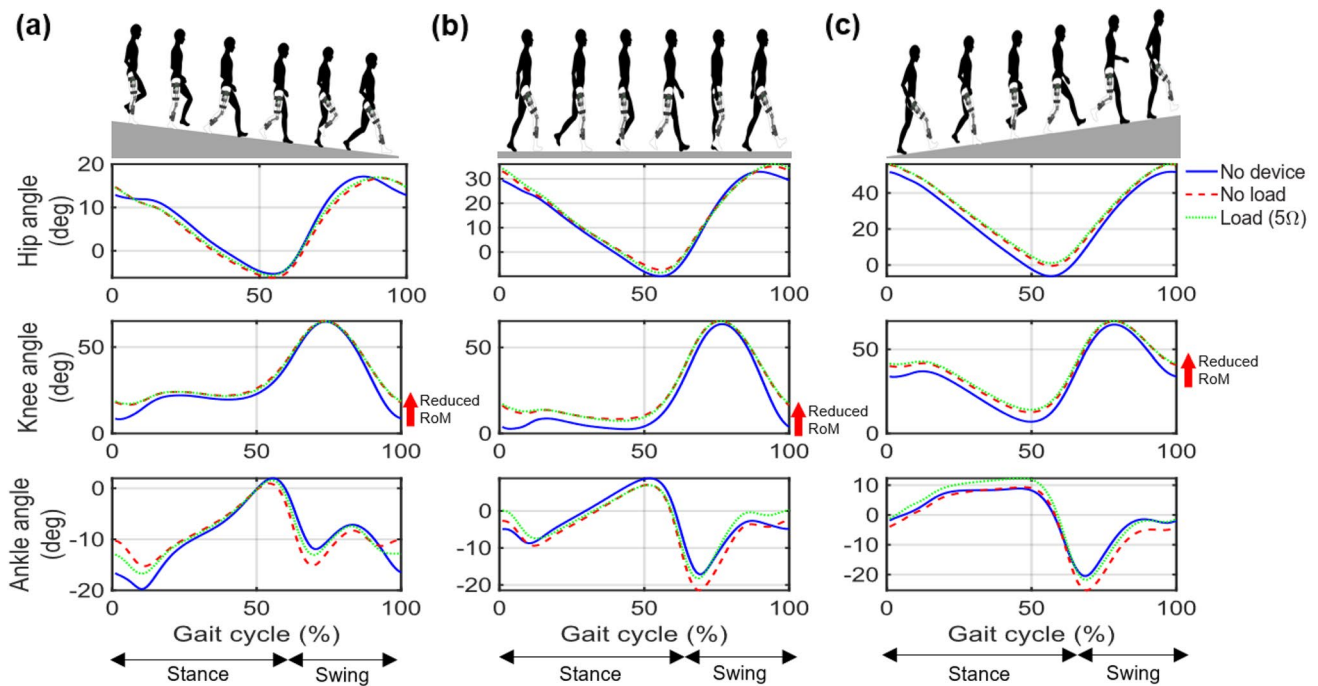


Fig. 10 Joint kinematics over the stride from heel strike (0%) to heel strike (100%); **a** downhill walking, **b** level-ground walking, and **c** uphill walking

owing to the braking torque of the harvester, as in previous studies [29, 30]. The sum of the knee flexion torque produced by the hamstring and the device torque may be higher than that during normal walking [29]. Even in the stance phase, the knee joint was more flexed than in the no-device condition, and it was restored to a state similar to that in the no-device condition when entering the swing flexion phase. In the swing extension of downhill walking, the kinematic change was the same as that during level-ground walking. In the stance phase of the harvesting mode, the knee angle that was less extended in the previous swing phase was maintained until the stance started, and it followed the profile of normal gait without a significant change. During uphill walking, the knee maintained a more flexed state, as if the profile was shifted upward compared with normal walking, because it was mostly composed of the extension applied by the braking torque during the gait cycle.

The hip joint angle profile was not changed according to the harvester engagement in level-ground and downhill walking. However, the RoM of the hip joint decreased slightly owing to the flexion of the joint in uphill walking. This appeared to occur to compensate for the step length reduced by the joint angle of the knee to maintain the gait for climbing the incline. The step length and width did not have any significant change in other walking environments and harvester conditions. These two parameters can increase the metabolic cost when deviating from the optimal conditions [56]. Although the designed BRBEH did not impose a

penalty on gait owing to the change in step length or width, the metabolic cost may increase owing to the change in kinematics [30].

The muscle activity was calculated as the average of the muscle signals of the entire gait cycle. To check the effectiveness of the harvester on the muscles, the average EMG signals of swing extension (70–100%) on level-ground/downhill walking and stance extension (0–30%) on uphill walking were separately observed in addition to the average signal during the entire gait. These periods are the phases in which the braking torque primarily acts. The measurement results for the hamstring and quadriceps muscle groups are presented in Figs. 11 and 12, respectively.

In the swing extension phase of level-ground walking, the semitendinosus activity of the hamstrings was decreased up to 27% compared with that during normal walking, showing a significant difference in the load condition, as shown in Fig. 11b. However, the biceps femoris showed increased activity compared with that during normal walking. This appears to be due to the mispositioning of the EMG sensor, rather than the braking torque from the harvester. The brace fixing of the harvester interfered with the electrode attachment position of the biceps femoris. Thus, the electrode position was slightly adjusted from the recommended position [57]. In addition, as the muscle was closest to the installation position of the harvester, there may have been an increase in activity owing to the carrying mass or pressure from the harvester. The tendency of

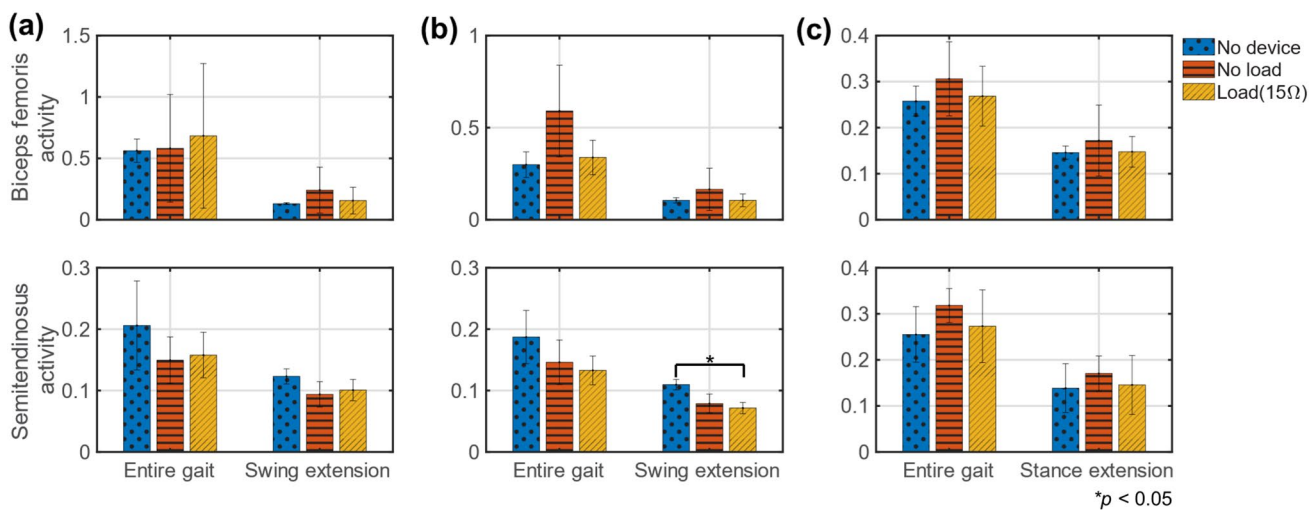


Fig. 11 Average hamstring muscle activity; a downhill walking, b level-ground walking, and c uphill walking

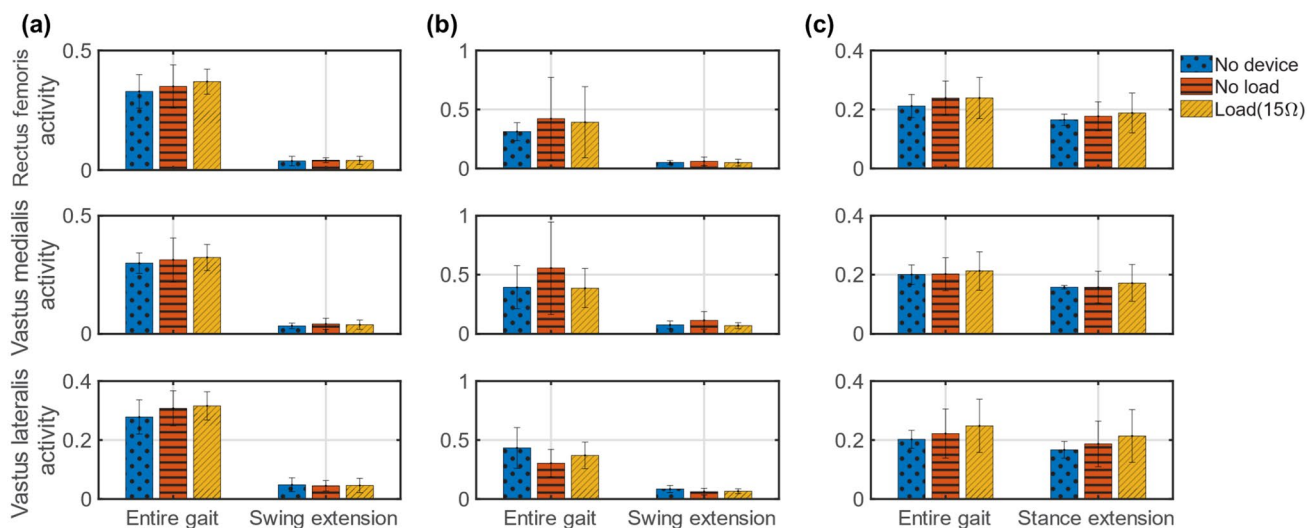


Fig. 12 Average quadriceps muscle activity; a downhill walking, b level-ground walking, and c uphill walking

the biceps femoris activity to increase when the harvester was equipped was also observed during sloped walking.

Negative work assistance through wearable devices is much more difficult than positive work assistance and requires sophisticated control. The eccentric contraction of muscles in negative work is already more efficient than the concentric contraction in positive work [58]. In addition to the muscles, negative work is supported by the energy return mechanism of soft tissues. If the harvester interferes with this mechanism, the activity of the antagonist muscle can be increased to ensure joint stability in response to the device [45]. However, there was no significant difference in the quadriceps activity during level-ground walking, as

shown in Fig. 12b. The designed harvester did not interfere with the natural energy return mechanism.

The change in the semitendinosus muscle activity during downhill walking was the same as that during level-ground walking, showing a slight decrease in the swing extension phase, as shown in Fig. 11a. By contrast, the activity of the quadriceps muscles slightly increased during downhill walking, as shown in Fig. 12a. Unlike walking on level ground, downhill walking requires strong negative work by the quadriceps for mass acceptance from the start of the stance [59]. Owing to the braking torque of the harvester, the downhill gait started with the knee flexed more than that in the normal gait. This flexion

pre-stretched the quadriceps muscle, which in turn disturbed the eccentric contraction.

Both hamstring and quadriceps muscle movements increased during uphill walking, as shown in Figs. 11c and 12c. When the ipsilateral leg moves in the stance phase, the primary muscle for the vertical propulsion of the body is the quadriceps muscle [59, 60]. At this time, the braking torque of the harvester would be a burden on the quadriceps, resulting in an average increase in the muscle activity by 10%. The hamstring acts as a hip extensor in the gait cycle, and its activity increases because a larger hip extension is required in inclined gait [61]. Although the designed harvester does not apply a direct moment to the hip joint, the dynamics of braking torque, such as the inertial effect, may interfere with the role of the hamstring as a hip extensor. The results of an EMG experiment with increased muscle activity during uphill walking showed the limitations of the harvester based on the one-way clutch.

The limitations of human testing, other than the structural problems of harvesters, should also be mentioned. Owing to the COVID-19 pandemic, we were unable to recruit sufficient participants to ensure statistical significance. In addition to the error owing to the positioning of the EMG sensor electrode mentioned above, the marker-based motion capture system may have caused kinematic errors owing to soft tissue artifacts, such as skins [62]. An analysis of the COH, TCOH, joint moment, and joint power was not possible owing to the lack of equipment. Experimental analyses of various slopes and walking speeds were also not performed.

4.4 Performance Comparison and Improvements

Table 4 shows the results of performance comparison with previous knee-joint-driven passive-type BRBEHs, which had the same configuration as the prototype. As the operating conditions of each harvester are different, it is difficult to compare the power density accurately. For example, some

studies extended the harvesting period from knee extension to flexion. In addition, the walking speed in this study was 1.2 m/s, which was slightly lower than that in other studies (1.5 m/s); hence, the amount of power generation may decrease. Nevertheless, the designed harvester has a high power density compared with other harvesters without a special mechanism. The results show that the BRBEH can be designed to have a high power density under the given design conditions through the proposed systematic design process.

Furthermore, it is possible to achieve higher power densities of BRBEH than the current state by modeling and design improvements. First, delay effect of one-way clutch and friction torque should be reflected in the modeling. The delay effect can be simulated by applying time delay function to the angular velocity (ω_h) of the human joint in Eqs. (14) and (15). Instead of predicting the delay time by modeling, clutch testing could be performed experimentally. Although modelling all the friction torque for mechanical components, such as clutch, bearings and belt, is complicated, at least the overall friction can be modeled by simplifying it as a function proportional to joint velocity. Second, the experimental results of joint kinematics change should be applied to the joint profile in the model. In the results of this study and previous studies, the angular velocity of the joint where the braking torque acts is generally lowered. To reflect this change of angular velocity, the maximum and minimum values of the velocity profile can be adjusted by multiplying the reduced velocity ratio obtained in the experiment. Furthermore, if the dynamics of the human body are analyzed using a musculoskeletal model, the BRBEH can be designed more precisely by predicting the kinematics of the joint [63]. Lastly, the linkage and brace connecting the human body and the harvester should be improved to secure wearability and transmit joint torque more accurately. This improvement aims to increase mechanical coupling efficiency (η_c), which is the critical flaw of the current prototype.

Table 4 Performance comparison with previous knee-joint-driven passive-type BRBEHs

Research	Device mass (kg)	Average harvested power (W)	Power density (W/kg)	Assistance timing
Li et al. [29]	1.6	4.8 ^L	3 ^L	Swing extension
Shepetyky et al. [30]	2.7	5.2 ^L	1.9 ^L	Swing extension
Cervera et al. [34]	1.5	6 ^L	4 ^L	Swing extension
Fan et al. [40]	1.8	4.1 ^L	2.3 ^L	Flexion and extension
Wu et al. [47]	0.54	5.4 ^L /6.5 ^D	10 ^L /12 ^D	Flexion and extension
This study*	0.98	3.2 ^L /0.4 ^U /2.5 ^D	3.3 ^L /0.4 ^U /2.6 ^D	Swing extension

*Device testing results

L Level-ground walking, *U* Uphill walking, *D* Downhill walking

5 Conclusion

In this study, a systematic analysis of the BRBEH was performed. Based on previous studies, the functional characteristics of the BRBEH system elements were reviewed. Subsequently, a design process that can reflect the characteristics of each component was suggested, and the harvester prototype was designed according to the design process. Several important design considerations were identified. To reduce the effect of the inertia of the BRBEH, a generator with low inertia needs to be selected rather than designing a low-inertia transmission. A high generator constant is advantageous in terms of power generation; however, if the constant is too high, it may be difficult to secure sufficient braking torque for gait assistance and high device efficiency simultaneously. Our harvester prototype was designed to have a high power density of 3.3 W/kg, simultaneously generating a braking torque of 8 N·m and an electrical power of 3 W in the device testing. Finally, the effect of harvesters on human biomechanics were analyzed through human testing. In particular, the effectiveness of the harvesters in sloped walking, which has not been explored in previous studies, was verified.

For more sophisticated energy harvesters, there is still a lack of information on the dynamics of the energy harvester and the interaction between the device and human. We showed that the dynamics of the energy harvester can affect the performance and can be considered in the design process. However, there exists a discrepancy in power estimation owing to friction and play in the transmission and slack in the braces. Moreover, the device may change the biomechanics of the human gait, resulting in an unexpected performance. Our results suggested that more tailored analytical models and optimization processes are required. Second, the device itself must be improved. Although we improved wearability by placing the core elements close to the center of mass of the human body and fixing them using a flexible cuff, there were still structural limitations that adversely affected walking. The misalignment of the knee joint and harvester reduced the mechanical coupling efficiency and caused discomfort. The additional metabolic cost incurred by carrying a total mass of 2 kg would also be a burden to normal human activities. In addition, the use of a one-way clutch interferes with the muscles during uphill walking. Future harvesters could be developed into anthropomorphic driving mechanisms that embody human knee movement with a compact and lightweight structure. Finally, our human testing result of sloped walking indicated the need for an adaptive control strategy that can adjust the on–off braking torque according to the gait environment. Hence, customized BRBEH control electronic circuits will be crucial in overcoming the functional limitations of current BRBEHs.

Supplementary Information The online version contains supplementary material available at <https://doi.org/10.1007/s40684-022-00472-6>.

Acknowledgements This study was supported by a National Research Foundation of Korea (NRF) grant funded by the Korean government (MSIT) (No. 2019R1C1C1006067).

Declarations

Conflict of interest On behalf of all the authors, the corresponding author states that there are no conflicts of interest.

References

- Choi, Y. M., Lee, M. G., & Jeon, Y. (2017). Wearable biomechanical energy harvesting technologies. *Energies*, *10*(10), 1483.
- Khalid, S., Raouf, I., Khan, A., Kim, N., & Kim, H. S. (2019). A review of human-powered energy harvesting for smart electronics: Recent progress and challenges. *International Journal of Precision Engineering and Manufacturing Green Technology*, *6*(4), 821–851.
- Starner, T., & Paradiso, J. A. (2004). Human generated power for mobile electronics. *Low Power Electronics Design*, *45*, 1–35.
- Nozariasbmarz, A., Collins, H., Dsouza, K., Polash, M. H., Hossaini, M., Hyland, M., & Vashaee, D. (2020). Review of wearable thermoelectric energy harvesting: From body temperature to electronic systems. *Applied Energy*, *258*, 114069.
- Yang, Y., Hu, H., Chen, Z., Wang, Z., Jiang, L., Lu, G., & Chen, Y. (2020). Stretchable nanolayered thermoelectric energy harvester on complex and dynamic surfaces. *Nano Letters*, *20*(6), 4445–4453.
- Ren, W., Sun, Y., Zhao, D., Aili, A., Zhang, S., Shi, C., & Yang, R. (2021). High-performance wearable thermoelectric generator with self-healing, recycling, and Lego-like reconfiguring capabilities. *Science Advances*, *7*(7), eabe0586.
- Lv, H., Liang, L., Zhang, Y., Deng, L., Chen, Z., Liu, Z., & Chen, G. (2021). A flexible spring-shaped architecture with optimized thermal design for wearable thermoelectric energy harvesting. *Nano Energy*, *88*, 106260.
- Riemer, R., & Shapiro, A. (2011). Biomechanical energy harvesting from human motion: Theory, state of the art, design guidelines, and future directions. *Journal of Neuroengineering and Rehabilitation*, *8*(1), 1–13.
- Liu, Y., Khanbareh, H., Halim, M. A., Feeney, A., Zhang, X., Heidari, H., & Ghannam, R. (2021). Piezoelectric energy harvesting for self-powered wearable upper limb applications. *Nano Select*, *2*(8), 1459–1479.
- Zou, Y., Raveendran, V., & Chen, J. (2020). Wearable triboelectric nanogenerators for biomechanical energy harvesting. *Nano Energy*, *77*, 105303.
- Yan, B., Yu, N., Zhang, L., Ma, H., Wu, C., Wang, K., & Zhou, S. (2020). Scavenging vibrational energy with a novel bistable electromagnetic energy harvester. *Smart Materials and Structures*, *29*(2), 025022.
- Wu, Z., Tang, J., Zhang, X., & Yu, Z. (2017). An energy harvesting bracelet. *Applied Physics Letters*, *111*(1), 013903.
- Chen, S., Xu, H., Liu, D., Hu, B., & Wang, H. (2014). A vision of IoT: Applications, challenges, and opportunities with china perspective. *IEEE Internet of Things Journal*, *1*(4), 349–359.
- Reid, R. C., & Mahub, I. (2020). Wearable self-powered biosensors. *Current Opinion in Electrochemistry*, *19*, 55–62.

15. Cristiani, J. (2008). The Current Status of Fuel Cell Technologies for Portable Military Applications. In: *25th International Battery Seminar and Exhibit, Fort Lauderdale, USA*
16. Wang, F., Gao, C., Kuklane, K., & Holmér, I. (2010). A review of technology of personal heating garments. *International Journal of Occupational Safety and Ergonomics*, 16(3), 387–404.
17. Laschowski, B., Razavian, R. S., & McPhee, J. (2021). Simulation of stand-to-sit biomechanics for robotic exoskeletons and prostheses with energy regeneration. *IEEE Transactions on Medical Robotics and Bionics*, 3(2), 455–462.
18. Sup, F., Varol, H. A., Mitchell, J., Withrow, T. J., & Goldfarb, M. (2009). Preliminary evaluations of a self-contained anthropomorphic transfemoral prosthesis. *IEEE/ASME Transactions on Mechatronics*, 14(6), 667–676.
19. Collins, S. H., & Kuo, A. D. (2010). Recycling energy to restore impaired ankle function during human walking. *PLoS One*, 5(2), e9307.
20. Collins, S. H., Wiggin, M. B., & Sawicki, G. S. (2015). Reducing the energy cost of human walking using an unpowered exoskeleton. *Nature*, 522(7555), 212–215.
21. Hyun, D. J., Bae, K., Kim, K., Nam, S., & Lee, D. H. (2019). A light-weight passive upper arm assistive exoskeleton based on multi-linkage spring-energy dissipation mechanism for overhead tasks. *Robotics and Autonomous Systems*, 122, 103309.
22. Kashiri, N., Abate, A., Abram, S. J., Albu-Schaffer, A., Clary, P. J., Daley, M., & Tsagarakis, N. (2018). An overview on principles for energy efficient robot locomotion. *Frontiers in Robotics and AI*, 5, 129.
23. Yu, S., Huang, T. H., Yang, X., Jiao, C., Yang, J., Chen, Y., & Su, H. (2020). Quasi-direct drive actuation for a lightweight hip exoskeleton with high backdrivability and high bandwidth. *IEEE/ASME Transactions on Mechatronics*, 25(4), 1794–1802.
24. Yu, S., Huang, T. H., Wang, D., Lynn, B., Sayd, D., Silivanov, V., & Su, H. (2019). Design and control of a high-torque and highly backdrivable hybrid soft exoskeleton for knee injury prevention during squatting. *IEEE Robotics and Automation Letters*, 4(4), 4579–4586.
25. Seok, S., Wang, A., Chuah, M. Y., Hyun, D. J., Lee, J., Otten, D. M., & Kim, S. (2014). Design principles for energy-efficient legged locomotion and implementation on the MIT cheetah robot. *IEEE/ASME Transactions on Mechatronics*, 20(3), 1117–1129.
26. Hitt, J. K., Sugar, T. G., Holgate, M., & Bellman, R. (2010). An active foot-ankle prosthesis with biomechanical energy regeneration. *Journal of Medical Devices*. <https://doi.org/10.1115/1.4001139>
27. Feng, Y., Mai, J., Agrawal, S. K., & Wang, Q. (2020). Energy regeneration from electromagnetic induction by human dynamics for lower extremity robotic prostheses. *IEEE Transactions on Robotics*, 36(5), 1442–1451.
28. Warner, H., Khalaf, P., Richter, H., Simon, D., Hardin, E., & van den Bogert, A. J. (2022). Early evaluation of a powered transfemoral prosthesis with force-modulated impedance control and energy regeneration. *Medical Engineering Physics*, 100, 103744.
29. Donelan, J. M., Li, Q., Naing, V., Hoffer, J. A., Weber, D. J., & Kuo, A. D. (2008). Biomechanical energy harvesting: Generating electricity during walking with minimal user effort. *Science*, 319(5864), 807–810.
30. Shepertycky, M., & Li, Q. (2015). Generating electricity during walking with a lower limb-driven energy harvester: Targeting a minimum user effort. *PLoS One*, 10(6), e0127635.
31. Li, Q., Naing, V., & Donelan, J. M. (2009). Development of a biomechanical energy harvester. *Journal of Neuroengineering and Rehabilitation*, 6(1), 1–12.
32. Martin, J. P., Shepertycky, M., Liu, Y. F., & Li, Q. (2016). Lower limb-driven energy harvester: Modeling, design, and performance evaluation. *Journal of Medical Devices*. <https://doi.org/10.1115/1.4033014>
33. Martin, J. P., & Li, Q. (2017). Overground vs. treadmill walking on biomechanical energy harvesting: An energetics and EMG study. *Gait & Posture*, 52, 124–128.
34. Cervera, A., Rubinshtein, Z. E., Gad, M., Riemer, R., & Peretz, M. M. (2016). Biomechanical energy harvesting system with optimal cost-of-harvesting tracking algorithm. *IEEE Journal of Emerging and Selected Topics in Power Electronics*, 4(1), 293–302.
35. Selinger, J. C., & Donelan, J. M. (2015). Myoelectric control for adaptable biomechanical energy harvesting. *IEEE Transactions on Neural Systems and Rehabilitation Engineering*, 24(3), 364–373.
36. Chen, C., Chau, L. Y., & Liao, W. H. (2017). A knee-mounted biomechanical energy harvester with enhanced efficiency and safety. *Smart Materials and Structures*, 26(6), 065027.
37. Ikawa, Y., Kobayashi, T., & Matsubara, T. (2018). Biomechanical energy harvester with continuously variable transmission: Prototyping and preliminary evaluation. In: *2018 IEEE/ASME International Conference on Advanced Intelligent Mechatronics (AIM)*, IEEE, (pp. 1045–1050).
38. Kobayashi, T., Ikawa, Y., & Matsubara, T. (2022). Sample-efficient gear-ratio optimization for biomechanical energy harvester. *International Journal of Intelligent Robotics and Applications*, 6(1), 10–22.
39. Cai, M., Liao, W. H., & Cao, J. (2018). A smart harvester for capturing energy from human ankle dorsiflexion with reduced user effort. *Smart Materials and Structures*, 28(1), 015026.
40. Fan, J., Xiong, C. H., Huang, Z. K., Wang, C. B., & Chen, W. B. (2019). A lightweight biomechanical energy harvester with high power density and low metabolic cost. *Energy Conversion and Management*, 195, 641–649.
41. Xie, L., Li, X., Cai, S., Huang, G., & Huang, L. (2019). Knee-braced energy harvester: Reclaim energy and assist walking. *Mechanical Systems and Signal Processing*, 127, 172–189.
42. Xie, L., Huang, G., Huang, L., Cai, S., & Li, X. (2019). An unpowered flexible lower limb exoskeleton: Walking assisting and energy harvesting. *IEEE/ASME Transactions on Mechatronics*, 24(5), 2236–2247.
43. Liu, M., Hill, C., Queen, R., & Zuo, L. (2021). A lightweight wearable biomechanical energy harvester. *Smart Materials and Structures*, 30(7), 075032.
44. Chan, H. H. T., Gao, F., Chung, B. L. H., Liao, W. H., & Cao, J. (2021). Knee energy harvester with variable transmission to reduce the effect on the walking gait. *Smart Materials and Structures*, 30(8), 085024.
45. Shepertycky, M., Burton, S., Dickson, A., Liu, Y. F., & Li, Q. (2021). Removing energy with an exoskeleton reduces the metabolic cost of walking. *Science*, 372(6545), 957–960.
46. Ren, L., Cong, M., Zhang, W., & Tan, Y. (2021). Harvesting the negative work of an active exoskeleton robot to extend its operating duration. *Energy Conversion and Management*, 245, 114640.
47. Wu, X., Cao, W., Yu, H., Zhang, Z., Leng, Y., & Zhang, M. (2022). Generating electricity during locomotion modes dominated by negative work via a knee energy-harvesting exoskeleton. *IEEE/ASME Transactions on Mechatronics*. <https://doi.org/10.1109/TMECH.2022.3157848>
48. Schertzer, E., & Riemer, R. (2014). Metabolic rate of carrying added mass: A function of walking speed, carried mass and mass location. *Applied Ergonomics*, 45(6), 1422–1432.
49. Zelik, K. E., & Kuo, A. D. (2010). Human walking isn't all hard work: Evidence of soft tissue contributions to energy dissipation and return. *Journal of Experimental Biology*, 213(24), 4257–4264.
50. Nuckols, R. W., Takahashi, K. Z., Farris, D. J., Mizrachi, S., Riemer, R., & Sawicki, G. S. (2020). Mechanics of walking and running up and downhill: A joint-level perspective to guide design of lower-limb exoskeletons. *PLoS One*, 15(8), e0231996.

51. Maxon Motors, (2021). EC 45 Flat, Brushless, Maxon Motors, Switzerland, Accessed 12 Dec 2021
52. Dickson, A. J., Burton, S., Shepetycky, M., Liu, Y. F., & Li, Q. (2015). Digitally controlled energy harvesting power management system. *IEEE Journal of Emerging and Selected Topics in Power Electronics*, 4(1), 303–317.
53. Bovi, G., Rabuffetti, M., Mazzoleni, P., & Ferrarin, M. (2011). A multiple-task gait analysis approach: Kinematic, kinetic and EMG reference data for healthy young and adult subjects. *Gait & Posture*, 33(1), 6–13.
54. NTN, Clutches (2022). <https://www.ntnglobal.com/en/products/catalog/pdf/2900E.pdf>, Accessed 14 Mar 2022
55. Insall, J. N., Binazzi, R., Soudry, M., & Mestriner, L. A. (1985). Total knee arthroplasty. *Clinical Orthopaedics and Related Research*, 192, 13–22.
56. Donelan, J. M., Kram, R., & Kuo, A. D. (2002). Mechanical work for step-to-step transitions is a major determinant of the metabolic cost of human walking. *Journal of Experimental Biology*, 205(23), 3717–3727.
57. Hermens, H., & Freriks, B. (1997). *The state of the art on sensors and sensor placement procedures for surface electromyography: a proposal for sensor placement procedures*. Enschede: Roessingh Research and Development.
58. Margaria, R. (1968). Positive and negative work performances and their efficiencies in human locomotion. *Internationale Zeitschrift für angewandte Physiologie einschließlich Arbeitsphysiologie*, 25(4), 339–351.
59. Pickle, N. T., Grabowski, A. M., Auyang, A. G., & Silverman, A. K. (2016). The functional roles of muscles during sloped walking. *Journal of Biomechanics*, 49(14), 3244–3251.
60. Harper, N. G., Wilken, J. M., & Neptune, R. R. (2018). Muscle function and coordination of stair ascent. *Journal of Biomechanical Engineering*. <https://doi.org/10.1115/1.4037791>
61. Franz, J. R., & Kram, R. (2012). The effects of grade and speed on leg muscle activations during walking. *Gait & posture*, 35(1), 143–147.
62. Hicks, J. L., Uchida, T. K., Seth, A., Rajagopal, A., & Delp, S. L. (2015). Is my model good enough? Best practices for verification and validation of musculoskeletal models and simulations of movement. *Journal of Biomechanical Engineering*. <https://doi.org/10.1115/1.4029304>
63. Seth, A., Hicks, J. L., Uchida, T. K., Habib, A., Dembia, C. L., Dunne, J. J., & Delp, S. L. (2018). OpenSim: Simulating musculoskeletal dynamics and neuromuscular control to study human and animal movement. *PLoS Computational Biology*, 14(7), e1006223.

Publisher's Note Springer Nature remains neutral with regard to jurisdictional claims in published maps and institutional affiliations.

Springer Nature or its licensor holds exclusive rights to this article under a publishing agreement with the author(s) or other rightsholder(s); author self-archiving of the accepted manuscript version of this article is solely governed by the terms of such publishing agreement and applicable law.



Kyung-Taek Yoon received the B.S. and M.S. degrees in mechanical engineering from Ajou University, Republic of Korea, in 2017 and 2019, respectively. He is currently working toward a Ph.D. degree at the same university. His current research interests include high-performance mechatronic systems, novel actuation and sensing devices, and wearable exoskeletons.



Young-Man Choi received the B.S., M.S., and Ph.D. degrees from the Department of Mechanical Engineering of Korea Advanced Institute of Science and Technology (KAIST), Republic of Korea, in 2002, 2004, and 2008, respectively. From 2008 to 2011, he worked at the National Institute of Standards and Technology (NIST), United States, and from 2012 to 2016, he was a senior researcher at Korea Institute of Machinery and Materials (KIMM), Daejeon, Republic of Korea. He is currently an associate professor in the Department of Mechanical Engineering at Ajou University, Suwon, Republic of Korea. His research interests include high-precision machines, roll-to-roll printing machines, and wearable biomechanical devices.